Journal of
Materials Chemistry A

Synthesis, crystal structure, and properties of stoichiometric hard tungsten tetraboride, WB_4

Journal:	*Journal of Materials Chemistry A*
Manuscript ID	TA-ART-03-2022-002268.R1
Article Type:	Paper
Date Submitted by the Author:	27-Jul-2022
Complete List of Authors:	Bykova, Elena; University of Bayreuth, Bayerisches Geoinstitut; Carnegie Institution of Washington, Earth and Planets Laboratory Ovsyannikov, Sergey; University of Bayreuth, Bayerisches Geoinstitut Bykov, Maxim; University of Cologne Institute of Inorganic Chemistry; Carnegie Institution for Science, Earth and Planets Laboratory Yin, Yuqing; University of Bayreuth, Materials Physics and Technology at Extreme Conditions, Laboratory of Crystallography; Shandong University, State Key Laboratory of Crystal Materials Fedotenko, Timofey; Deutsches Elektronen-Synchrotron, Photon Science Holz, Hendrik; Friedrich-Alexander-Universität Erlangen-Nürnberg, Department of Materials Science and Engineering Gabel, Stefan; Friedrich-Alexander-Universität Erlangen-Nürnberg, Department of Materials Science and Engineering Merle, Benoit; Friedrich-Alexander-Universitat Erlangen-Nurnberg, Chariton, Stella; University of Chicago, Center for Advanced Radiation Sources Prakapenka, Vitali; univ. chicago Dubrovinskaia, Natalia ; University of Bayreuth, Laboratory of Crystallography; Linköping University, Department of Physics, Chemistry and Biology (IFM) Goncharov, Alexander F. AFG; Carnegie Institution of Washington, Earth and Planets Laboratory Dubrovinsky, Leonid; University of Bayreuth, Bayerisches Geoinstitut

Synthesis, crystal structure, and properties of stoichiometric hard tungsten tetraboride, WB_4

Elena Bykova,[1,2] Sergey V. Ovsyannikov,[1] Maxim Bykov,[3] Yuqing Yin,[4,5] Timofey Fedotenko[6], Hendrik Holz,[7] Stefan Gabel,[7] Benoit Merle,[7] Stella Chariton,[8] Vitali B. Prakapenka,[8] Natalia Dubrovinskaia,[4,9] Alexander F. Goncharov[2], and Leonid Dubrovinsky[1]

[1] Bayerisches Geoinstitut, University of Bayreuth, Universitätsstrasse 30, D-95447, Bayreuth, Germany

[2] Earth and Planets Laboratory, Carnegie Institution for Science, 5241 Broad Branch Road, NW, Washington DC, 20015, USA

[3] Institute of Inorganic Chemistry, University of Cologne, Greinstrasse 6, 50939 Cologne, Germany

[4] Material Physics and Technology at Extreme Conditions, Laboratory of Crystallography, University of Bayreuth, 95440 Bayreuth, Germany

[5] State Key Laboratory of Crystal Materials, Shandong University, Jinan 250100, China

[6] Photon Science, Deutsches Elektronen-Synchrotron, Notkestrasse 85, 22607 Hamburg, Germany

[7] Friedrich-Alexander-Universität Erlangen-Nürnberg, Department of Materials Science and Engineering, Institute I, Interdisciplinary Center for Nanostructured Films (IZNF), Cauerstr. 3, 91058 Erlangen, Germany

[8] Center for Advanced Radiation Sources, The University of Chicago, 5640 S. Ellis, Chicago, IL, 60637, USA

[9] Department of Physics, Chemistry and Biology (IFM), Linköping University, SE-58183 Linköping, Sweden

Abstract

Tungsten tetraboride has been known so far as a non-stoichiometric compound with a variable composition (e.g. WB_{4-x}, WB_{4+x}). Its mechanical properties could exceed those of hard tungsten carbide, which is widely used nowadays in technique and science. The existence of stoichiometric WB_4 has not been proven yet, and its structure and crystal chemistry remain debatable to date. Here we report the synthesis of single crystals of the stoichiometric WB_4 phase at high-pressure high-temperature conditions. The crystal structure of WB_4 was determined using synchrotron single-crystal X-ray diffraction. *In situ* high-pressure compressibility measurements show that the bulk modulus of WB_4 is 238.6(2) GPa for $B' = 5.6(0)$. Measurements of mechanical properties on bulk polycrystalline sub-millimeter size samples at ambient conditions reveal a hardness of ~36 GPa confirming that the material falls in the category of superhard materials.

Introduction

Inexpensive hard and superhard (with Vickers hardness around 40 GPa and above) materials are in much demand for various industrial applications. Novel carbides[1], nitrides[2–8], borides[9–23], and other compounds of transition metals[24,25], which can potentially combine high hardness and promising optical, electronic, and other properties, are the focus of extensive investigations[26–28]. Nowadays, one of the most widely used hard material for commercial applications is tungsten carbide, WC. This fact motivates investigations of other potentially hard tungsten compounds, primarily, borides[29–37]. Among them, a phase referred to "WB_4"[38–49], together with its several derivatives (e.g., $W_{1-x}B_3$, WB_{4-x}, WB_{4+x}, $WB_{4.2}$, and WB_{5-x})[50–56] were identified as highly promising candidates, whose mechanical characteristics (e.g. theoretical and experimental values of H_V vary from 30 to 45 GPa[26,44,45,47,49,54]) could exceed those of WC (Vickers hardness H_V ~18-20 GPa[57]). However, a crystal chemistry of the "WB_4" phase remains debatable during decades, and thus, often it is not clear what material is being considered in a particular publication.

Based on high-quality powder diffraction data, several probable structural models for the "WB_4" phase were suggested (hexagonal unit cell, a ~ 5.20 Å, c ~ 6.34 Å, Figure 1 a-d)[38,39,42–45,47,58]. In contrast, theoretical calculations suggested an alternative crystal structure for "WB_4" (sp.gr. $P6_3/mmc$, a ~ 2.93-2.96 Å, c ~ 10.9-11.0 Å, Figure 1 f)[31,36,37,48], but it was not experimentally observed to date.

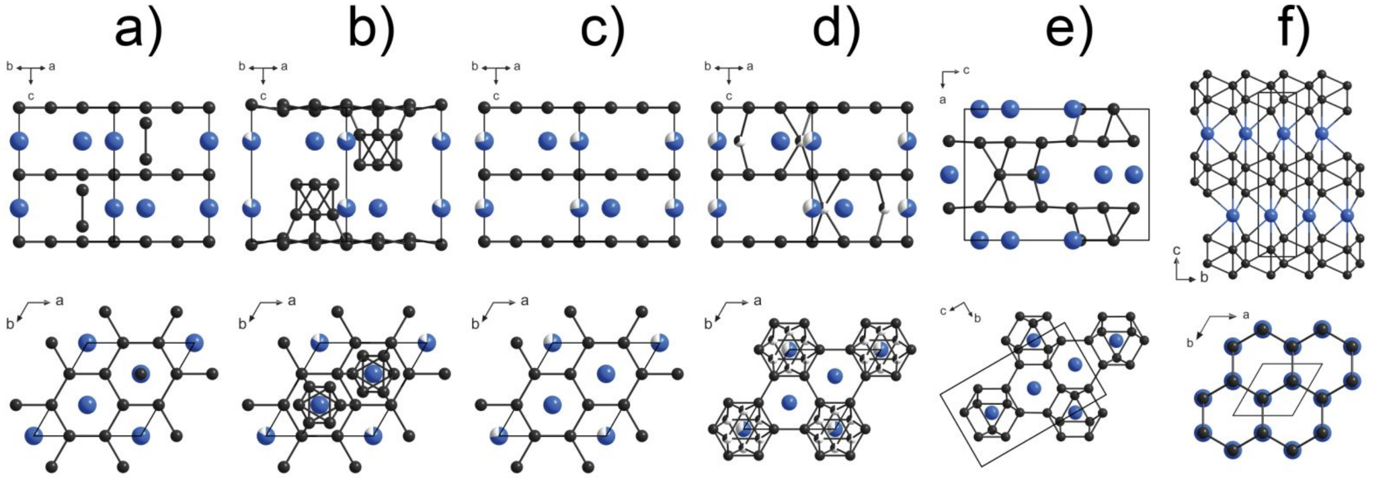

Figure 1. Various models of the crystal structure proposed for WB_4: (*a*) the crystal structure of WB_4 by Romans and Krug[39]; (*b*) $W_{1.83}B_9$ by Nowothy *et al.*[58]; (*c*) $W_{1-x}B_3$ following Lundström and Rosenberg[59] and Zeiringer *et al.*[42]; (*d*) $WB_{4.2}$ by Lech *et al.* [47]; (*e*) WB_5 by Kvashnin *et al.*[34,54]; (*f*) theoretically predicted stoichiometric WB_4[31,36,37,48]. The blue spheres represent tungsten atoms, the black spheres are boron atoms, and the partially filled spheres indicate defect B or W sites.

Recently, one more boron-rich phase, WB_5 was firstly predicted (sp. gr. $Pmmn$, $a = 6.369$, $b = 5.199$, $c = 8.993$ Å, Figure 1 e)[34], and then synthesized in the form of two boron-deficient phases, $WB_{4.18}$ and $WB_{4.86}$[54]. Crystal structures of these WB_5, $WB_{4.18}$ and $WB_{4.86}$ phases were found to be very similar to those reported earlier for the seemingly "WB_4" phase and its derivatives[38,39,42]. This finding may suggest that: (*i*) stoichiometric WB_5 phase is actually "parent" for the family of boron-deficient phases WB_{5-x} ($0 \leq x < 1.6$) reported to date; (*ii*) a genuine stoichiometric WB_4 phase for which a different crystal structure was predicted[31,36,37,48], probably has not been synthesized yet, and previous claims of its synthesis were likely due to a confusion with one of the WB_{5-x} phases[54].

In this work, we report a first synthesis of single crystals of the so far "elusive" stoichiometric WB_4 phase and an accurate determination of its crystal structure by single-crystal X-ray diffraction. In order to synthesize the phase we first performed a fast screening of chemical reactivity of W-B system up to 30 GPa and then scaled-up the amount of WB_4 phase in a multi-anvil apparatus. We find that a crystal structure of the genuine WB_4 phase indeed differs from previous experimentally-determined models for the seemingly "WB_4" phase[26,38,39,42,44,45,47,49,59], while, it is consistent well with a one predicted for WB_4[31,36,37,48]. Examinations of mechanical properties of the single- and polycrystalline samples of WB_4 confirm a hard nature of this phase.

Experimental procedures

Synthesis of WB_4 single crystals in diamond anvil cells

For high-pressure high-temperature experiments we have used a BX90 type DAC[60] equipped with Boehler-Almax diamonds with a 200 μm culet size (60° opening angle). In-between diamonds we placed a rhenium gasket pre-indented to 25 μm thickness with a hole of about 100 μm in diameter that served as a pressure chamber. Inside the pressure chamber, we placed a thin tungsten plate sandwiched between pre-compressed amorphous boron powder together with a small ruby sphere (for pressure estimation). Neon was used both as a pressure transmitting medium and as a pressure standard[61].

The laser-heating coupled with XRD measurements were conducted at the 13-IDD beamline at the Advanced Photon Source, Argonne National Laboratory (Pilatus CdTe 1M detector, x-ray wavelength $\lambda = 0.2952$ Å, focal spot ~3 μm)[62]. Sample-to-detector distance, coordinates of the beam center, tilt angle and tilt plane rotation angle of the detector images were calibrated using NIST LaB_6. Lasers were focused down to a flat top about 10 μm in diameter. The sample temperature was measured by the standard spectroradiometry method[63] using an Acton SP-2360 imaging spectrograph coupled with a PI-MAX3 1024i ICCD camera from Princeton Instruments. Pressure values and maximum heating temperatures are given in Table S1.

After each laser heating cycle, a detailed X-ray diffraction map was collected around the heated spot in order to determine the phase composition of the reaction product. At each pressure point, single-crystal XRD images were collected in different spots with the decent quality of the diffraction data (up to six data collection procedures) in order to determine phase composition of the reaction product. The single-crystal XRD images were recorded while rotating the sample about a single ω-axis from -30 to +30° in small steps of 0.5°.

DIOPTAS software[64] was used for preliminary phase analysis and calculation of pressures from the positions of the XRD lines of Ne. Powder XRD patterns were analyzed in JANA2020, where the unit cell parameters of the phases in the multi-phase mixtures were refined from full-profile Le Bail fit[65].

Synthesis of WB_4 single crystals in multi-anvil assemblies

The WB_4 samples were synthesized high-pressure high-temperature (HP-HT) conditions using multi-anvil presses at Bayerisches Geoinstitut (BGI)[66]. Typically, the samples were synthesized at 20 GPa under heating at 1800-2000 °C daring several hours (Table S1). We used standard multi-anvil assemblies with $LaCrO_3$-heaters and W3Re/W25Re thermocouples for temperature determination. Sample capsules were prepared from a 50-μm thick tungsten foil (99.95 % purity, HMW Hauner GmbH & Co.KG company). We followed several synthetic routes, including mixing of fine powders of tungsten of boron and mixing of tungsten foils with boron powder. The latter allowed to fabricate microscopic single crystals at the border of the tungsten foils; whereas, the former could fabricate relatively large polycrystals. Besides the above tungsten foil, we used tungsten powder (99.9 % purity, Chempur company) for mixing with boron powder. In preliminary testing syntheses, we used a powder of amorphous boron (95-97 % purity, Chempur company), while for synthesis of chemically pure samples we ground into powder the β-boron crystals (99.5% purity, Chempur company). Structural and chemical analyses of the samples were performed by X-ray diffraction using a three-circle Bruker diffractometer (SMART APEX CCD detector, Incoatec IμS 3.0 microfocus X-ray source, Ag-$K\alpha$ radiation), and by scanning electron microscopy (SEM) at a LEO-1530 instrument, respectively. Other details and procedures were similar to those described before[67,68].

Measurements of single-crystal compressibility

A single crystal of WB_4 (black, plate-shape, 10 x 10 x 5 μm^3) pre-selected at in-house single-crystal diffractometer was loaded in a membrane-driven BX90 type DAC equipped with Boehler-Almax diamonds with a 250 μm culet size (60° opening angle, Re gasket). A small ruby sphere as well as a Ne pressure-transmitting medium were used for pressure determination. The WB_4 crystal in the diamond anvil cell was compressed to about 54 GPa with a pressure step of 1-4 GPa. Single-crystal XRD of the sample was measured at each pressure point (narrow ω-scanning from -30 to +30°, 0.5° steps).

The XRD experiments were conducted at the Extreme Conditions Beamline P02.2 at PETRA III, Hamburg, Germany (Perkin Elmer XRD1621 flat panel detector, $\lambda = 0.2900$ Å, KB-mirror focusing, focal spot ~3 μm). Sample-to-detector distance, coordinates of the beam center, tilt angle and tilt plane rotation angle of the detector images were calibrated using CeO_2.

Single-crystal X-ray diffraction

Single-crystal XRD data (the unit cell determination, integration of the reflection intensities, empirical absorption correction) were processed using CrysAlisPro software[69]. In case of multi-phase and multi-grain samples (which, for instance, are being formed after laser heating), we manually searched for peaks belonging to the most intense grains using the reciprocal space Ewald explorer implemented in CrysAlisPro. After the unit cell indexing, the unit cell and orientation matrix obtained were used for further data integration.

A single crystal of orthoenstatite ($(Mg_{1.93},Fe_{0.06})(Si_{1.93},Al_{0.06})O_6$, *Pbca*, a = 18.2391(3), b = 8.8117(2), c = 5.18320(10) Å) was used to calibrate the instrument model of CrysAlisPro (the sample-to-detector distance, the detector's origin, offsets of the goniometer angles, rotation of the X-ray beam and the detector around the instrument axis).

The crystal structures were determined by SHELXT[70], a structure solution program that uses the method of intrinsic phasing. The crystal structure was refined against F^2 on all data by full-matrix least-squares with the SHELXL[71] software. SHELXT and SHELXL programs were implemented in Olex2 software package[72]. Since the body of the diamond anvil cell shadows more than 50% of the diffraction reflections, the reflection datasets were incomplete. In order to improve the data/parameter ratio, only atomic thermal parameters of tungsten were refined in anisotropic approximation. Another refinement strategy where boron atoms have been also refined anisotropically with RIGU rigid-bond restraint gave no significant improvements in R_1/wR_2 values, but rather brought a problem with elongated/negative ADPs for most B atoms, therefore it was not applied.

A detailed summary of the crystal structure refinements together with the unit cell parameters, atomic coordinates and isotropic displacement parameters are summarized in Table S2. The X-ray crystallographic coordinates have been deposited at the Inorganic Crystal Structure Database (ICSD), deposition numbers are given in Table S2. These data can be obtained from CCDC's and FIZ Karlsruhe's free service for viewing and retrieving structures (https://www.ccdc.cam.ac.uk/structures/).

Measurements of the hardness and Young's modulus

Nanoindentation was performed using a Nanoindenter G200 platform (KLA-Tencor, Milpitas, CA, USA), equipped with a Berkovich diamond tip (Synton MDP, Nidau, Switzerland) and featuring the continuous stiffness method (CSM)[73]. The indents were separated by a distance of at least 10 µm, so that their plastic zones did not overlap[74]. The indentations were performed on different areas of the sample, which respectively appeared homogeneous and heterogeneous in the optical micrographs as can be seen in Figure S1, and are assumed to be single crystalline and polycrystalline, the size of the single crystalline areas could reach 30 microns. All in all, 20 measurements were performed. For each test, loading was performed at a constant strain-rate of 0.1 s^{-1} up to a maximal indentation depth of at least 900 nm. A 2 nm large CSM oscillation superimposed at 41 Hz on the loading signal was used to continuously measure the hardness and Young's modulus with increasing indentation depth. The acquired data were evaluated using the Oliver–Pharr method[75,76]. To this purpose, the diamond punch geometry was calibrated in fused silica and the machine frame stiffness correction was refined so as to obtain a constant stiffness-squared-over-load ratio during indentation on the samples. The mechanical properties were averaged over the indentation depth range 700-900 nm in order to minimize tip blunting effects at shallow depth. The conversion of the reduced moduli to Young's moduli was performed assuming a Poisson's ratio of 0.2 for WB_4[74]. The conversion from the nanoindentation hardness H_{IT} to the Vickers hardness H_V was carried out with a factor 0.926[77].

Results and discussion

Synthesis of single crystals and polycrystals

Single and polycrystals of WB_4 were synthesized at high-pressure high-temperature (HP-HT) conditions using both large-volume multi-anvil presses at BGI, and laser-heated diamond anvil cells (DACs). In the experiments using the DAC, a WB_4 phase (sp.gr. $P6_3/mmc$, a = 2.8481(3) Å, c = 10.752(2) Å) was first

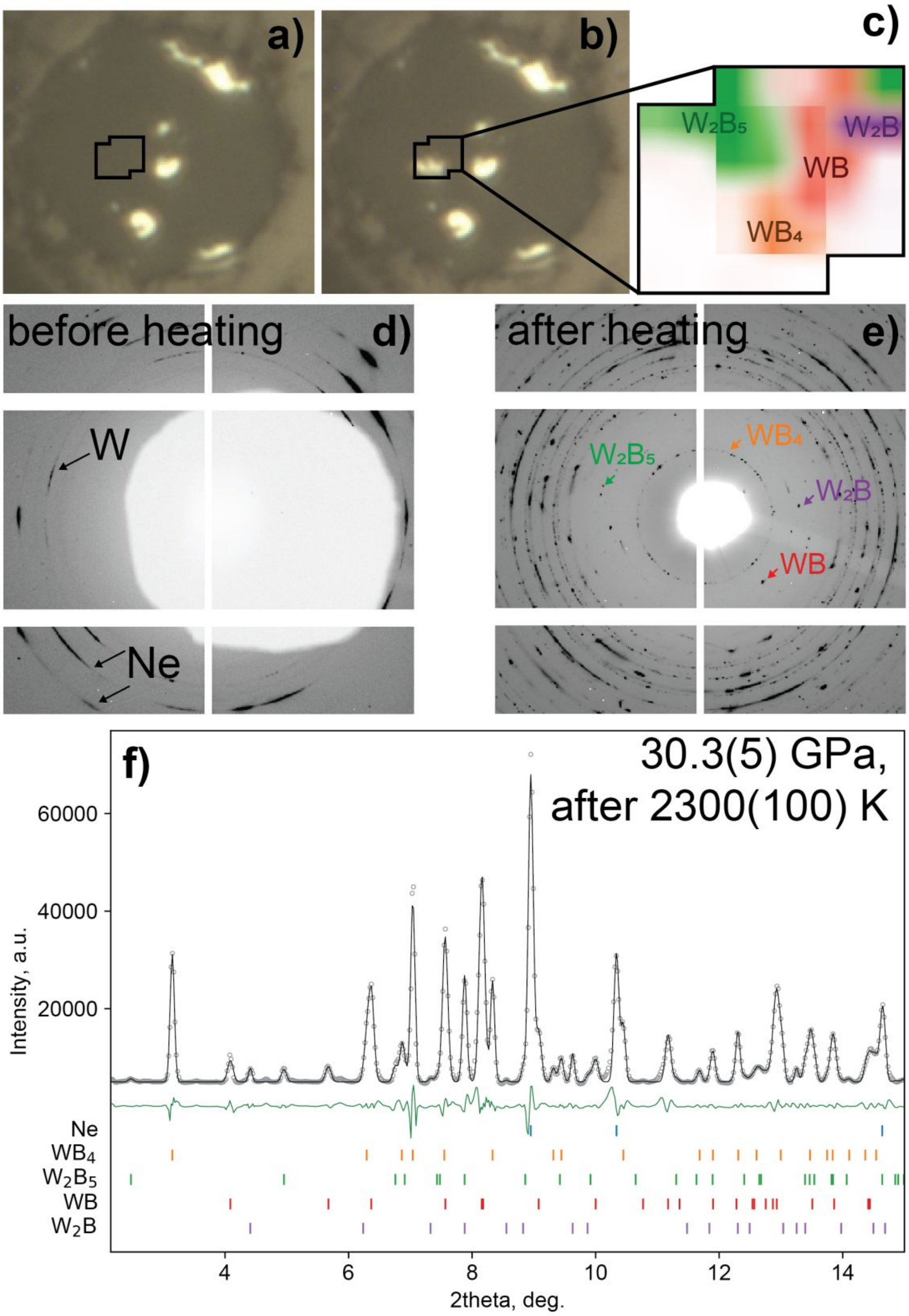

Figure 2. Synthesis of tungsten borides at high pressure. Microscopic images of the pressure chamber before (*a*) and after (*b*) the laser heating at 30.3(5) GPa, while the inset (*c*) shows phase distribution around the heated area obtained by X-ray diffraction mapping of the heated area. By using a combination of powder and single-crystal XRD methods, four borides of tungsten were identified in the pressure chamber, namely, WB_4, W_2B_5, WB and W_2B. Corresponding fragments of 2D diffraction images at the low-2θ region show diffraction peaks before (*~~a~~d*) and after a laser heating (*~~b~~e*). A white area at (*~~a~~d*) is a shadow from a beam stop to block scattering from X-ray transparent glassy carbon mirrors used for on-axis laser heating. The lower image (*~~c~~f*) shows a powder X-ray diffraction data collected at 30.3(5) GPa after the laser heating up to 2300(100) K (λ = 0.2952 Å): the experimental data are shown by grey circles (the background was subtracted), a Le Bail fit – by the black solid line, a difference curve –by the green solid line; the ticks show predicted positions of the diffraction peaks. Le Bail fit showing profiles of the individual phases is given in supplementary Figure S2.

detected at 30.3(5) GPa after a laser heating up to 2300(100) K. As can be seen from Figure 2, single crystals of WB_4 are formed together with a W_2B phase (sp.gr. *I*4/*mcm*, *a* = 5.4257(10) Å, *c* = 4.6189(12) Å), WB (sp.gr. $I4_1/amd$, *a* = 3.0325(4) Å, *c* = 16.558(3) Å), and a phase with a R-centered hexagonal unit cell (*a* = 2.9143(5)Å, *c* = 20.463(5) Å). The latter lattice parameters belong to a tungsten boride for which two chemical compositions have been proposed, namely, W_2B_5[78] and W_2B_4[79,80] (below we use W_2B_5 notation). Such a wide variety of the W:B ratios can be explained by a design of our DAC experiments. In the reaction chamber, a tungsten foil was embedded between two pieces of pre-compressed boron powder, which results in inhomogeneous distribution of the reactants across the reaction chamber and their insufficient mixing. More boron-rich borides likely formed in the spots with local excess of boron, while borides with larger W:B ratio formed in the boron-poor regions. We cannot exclude that thermal gradients typical to the laser heating (at least +-100 K) could lead to chemical variety of the resulting products.

In the multi-anvil experiments, tungsten tetraboride (as well as a byproduct, WB_2) can be successfully synthesized at 20 GPa and 2073 K. It should be noted that no WB_5 or any of its derivatives have been found among the reaction products neither in the multi-anvil nor in DAC experiments.

Crystal structure and comparison with previous results

From the synthesis products, we selected high-quality single crystals of WB_4 and determined their crystal structure by single-crystal X-ray diffraction (Figure S~~2~~3). In the crystal structure of tungsten tetraboride (Figure 3 a,b), the metal atoms form the flat hexagonal close packed layers perpendicular to *c*-axis that follow ABABA… sequence. Covalently-bonded boron networks are located between layers of tungsten atoms. The networks consist of two puckered layers connected through short B-B bonds (notated as *d*3 in Figure 3 a). Such layers are formed by condensed six-membered rings of boron in a chair-like conformation, which one can find, for example, in grey arsenic (A7-type) and in a high-pressure modification of black phosphorous (Figure 3 c)[81]. The crystal structure of WB_4 demonstrates a close similarity with one of hard ReB_2, which has the same arrangement of metal atoms, while, its boron network is formed only by a one puckered layer[82]. The single-crystal XRD data showed that tungsten and boron atoms fully occupy their positions, leaving no vacancies. The crystal structure we experimentally determined fully agrees with theoretical predictions[31,36,37,48].

Both early[38,39] and recent[26,42,44,45,47,49] experimental structural studies of the "WB_4" phase proposed a different crystal structure, which is built from interchanging defect close-packed metal layers and planar boron honeycomb layers, and interstitial boron atoms (Figure 1 a-e). A structural similarity with WB_5 suggests that all the "WB_4" phases reported in previous publications were, likely, boron-deficient WB_{5-x}, but not genuine stoichiometric WB_4[54]. Furthermore, it was predicted that genuine stoichiometric WB_4 phase is thermodynamically stable only above 1 GPa[54], and hence, ambient-pressure syntheses were unlikely to be capable to fabricate it.

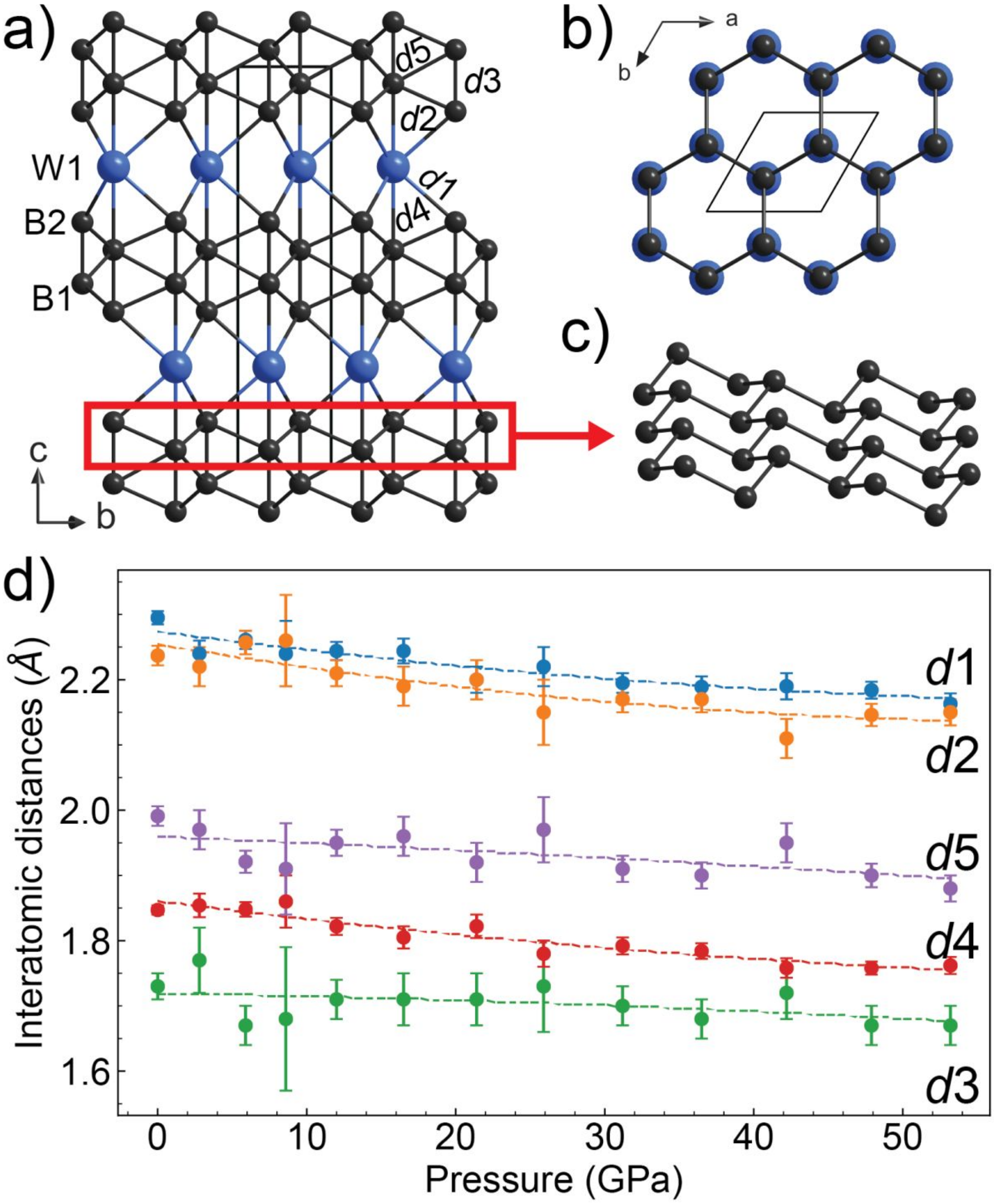

Figure 3. Crystal structure of WB_4 projected down the *a*-axis (*a*) and *c*-axis (*b*). All structures consist of hexagonal layers of W atoms (blue spheres) interchanging with network formed by covalently bonded boron atoms (black spheres). Red rectangle highlights a single puckered layer formed by condensed six-membered rings of boron in a chair-like conformation, the layer in a different projection is shown at (*c*). Compressibility of interatomic distances and bonds in WB_4 (*d*): *d*1, *d*2 – W…B distances, *d*3-*d*5 – B…B bonds. The solid

symbols – data retrieved from the single-crystal diffraction measurements, the dash lines are the 2nd polynomial fits of compression data serving as a guide to the eye.

Mechanical properties

We examined the mechanical properties of our WB_4 crystals by measurements of single-crystal compressibility using a pressure-dependent single crystal X-ray diffraction up to 54 GPa (Figure 4), and by measurements of both hardness and Young's modulus.

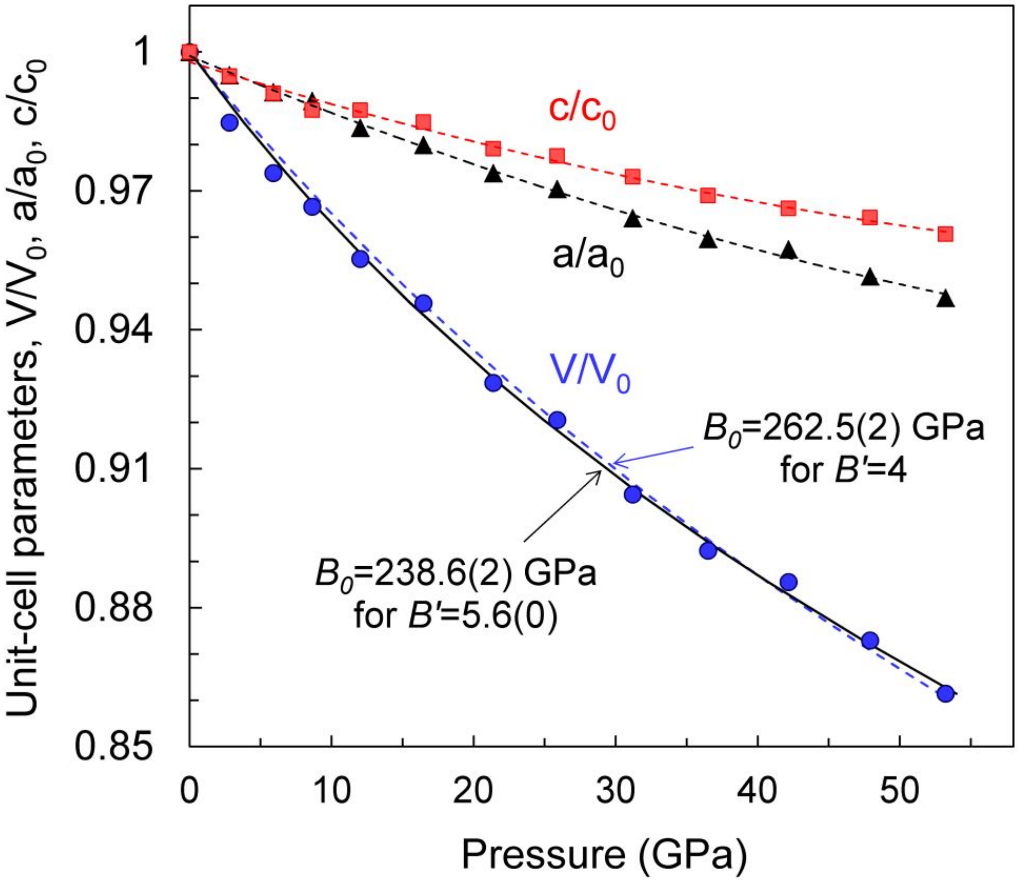

Figure 4. Pressure dependencies of relative variations in the unit-cell volume and lattice parameters of a WB_4 single crystal at 295 K. Error bars are smaller than symbols' size.

The high pressure *in situ* single crystal X-ray diffraction studies up to 54 GPa were carried out using a neon quasi-hydrostatic pressure-transmitting medium. A WB_4 sample showed no phase transitions under compression up to 54 GPa, and we could follow pressure evolutions of its unit cell parameters. Fitting the third-order Birch-Murnaghan equation of state to the volumetric data, we estimated a bulk modulus as $B_0 = 238.6(2)$ GPa for $B' = 5.6(0)$ and $B_0 = 262.5(2)$ GPa for fixed $B' = 4$ (Figure 4). As seen from this plot, the WB_4 crystal has a sizable difference in axial compressibility, and along *c*-axis, it is the most incompressible. The shortest B-B bonds (noted as *d*3 Figure 3 a) in the crystal structure are oriented along *c*-axis and have the lowest compressibility compared to the other B-B bonds and W…B contacts (Figure 3 d); therefore, we can expect that these bonds largely contribute to the axial incompressibility. The bulk modulus of WB_4 appeared to be smaller than that for WB_{5-x} phases: $B_0 \sim 304\text{-}342$ GPa with fixed $B' = 4$ (See Ref. [83] and refs therein). On the other hand, stoichiometric WB_4 shows no lattice parameter softening around 42 GPa, as has been observed previously for a non-stoichiometric phase[83].

The hardness and Young's modulus

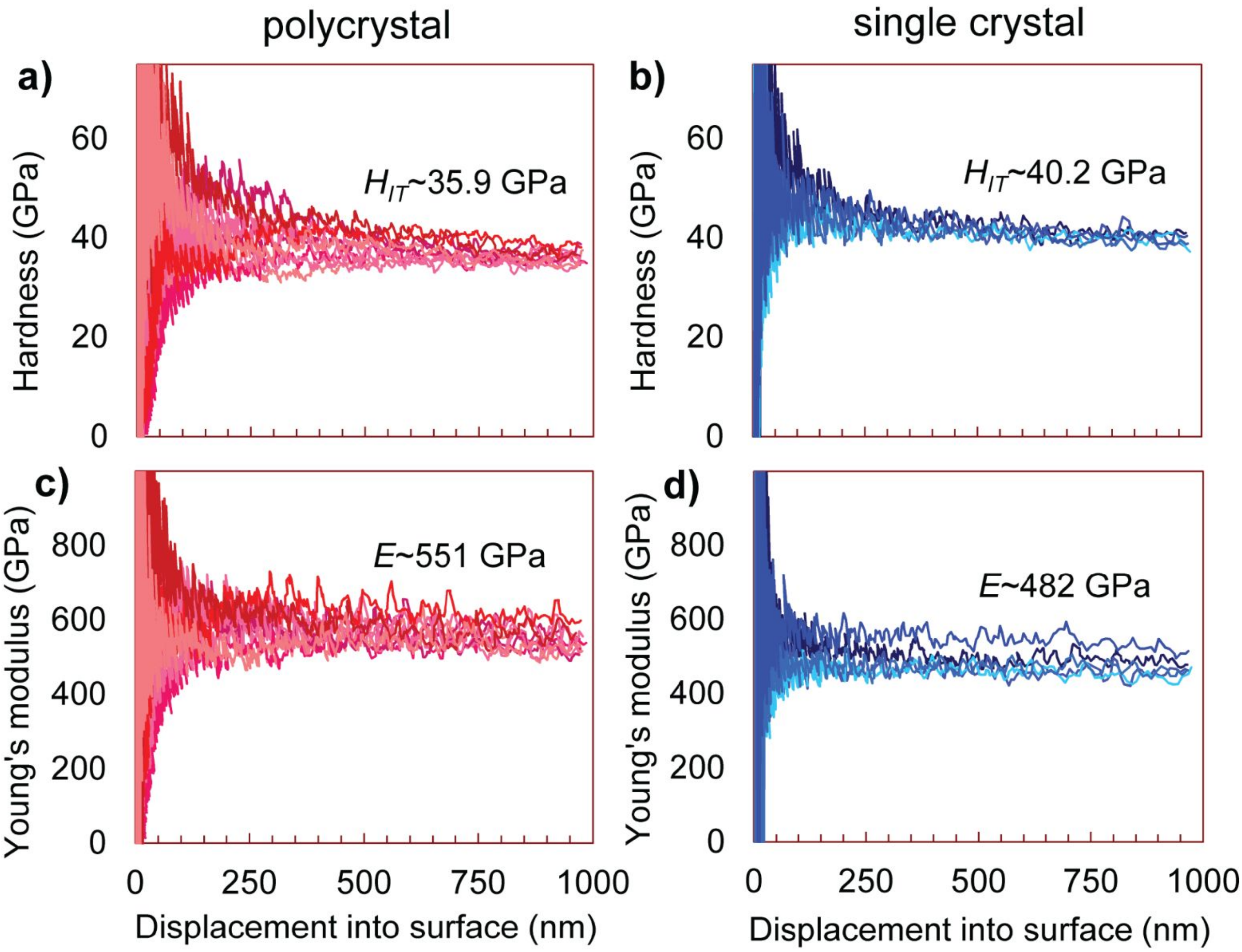

Figure 5. The nanoindentation hardness, H_{IT} (*a*, *b*) and Young's modulus, *E* (*c*, *d*) of polycrystal (*a*, *c*) and single crystal (*b*, *d*) of WB_4 at 295 K. Each plot combines several tests and shows average values.

The nanoindentation hardness and Young's modulus measurements are shown in Figure 5. In the likely single crystalline areas, they returned average values of $H_{IT} = 40.2(5)$ GPa (corresponding to $H_V = 37.3(5)$ GPa) and $E = 482(30)$ GPa. Likewise, for the likely polycrystalline area, the hardness was found to be $H_{IT} = 35.9(1.6)$ GPa (corresponding to $H_V = 33.3(1.5)$ GPa) and the Young's modulus $E = 551(24)$ GPa (Figure 5). These magnitudes confirm that WB_4 is a hard material, and generally agrees with previous experimental estimations of hardness for seemingly "WB_4" ($WB_{5\text{-}x}$) phases as about $H_V \sim$ 30-45 GPa[26,44,45,47,49,54] (see Table 1 for comparison of mechanical properties). The elastic and plastic properties of hard solids are known to correlate with each other[84]. Given the above experimentally-determined values of the bulk modulus ($B_0 = 262.5(2)$ for $B = 4$) (Figure 4) and hardness ($H_V = 37.3(5)$ and $33.3(1.5)$ GPa)(Figure 5 a,b) for single- and polycrystalline samples of WB_4, one can calculate their shear moduli (*G*) by using an empirical formula proposed by X. Q. Chen *et al.* and verified by numerous examples, as follows[85,86]:

$$H_V^{(Chen)} = 2(k^2G)^{0.585} - 3,$$

where $k=G/B_0$. The returned values of the shear moduli of $G = 227(2)$ and 214(5) GPa for single- and polycrystalline samples, respectively, are in a good agreement with the literature data (Table 1). The Pugh modulus ratios (B_0/G) are 1.16(1) and 1.23(3), respectively. These values are well less than 1.75, – the threshold magnitude, which differentiates between brittle ($B_0/G < 1.75$) and ductile ($B_0/G > 1.75$) materials[87]. Hence, WB_4 is a brittle material and cannot be deformed in a ductile manner.

Table 1. Mechanical properties of stoichiometric WB_4 (isotropic bulk modulus B, shear modulus G, Young's modulus E and estimated values of Vickers' hardness H_V, all units in GPa) compared with reported literature values for various models of WB_4, WB_5 and their derivatives.

Phase	**Space group**		***B***	***G***	***B*/*G***	***E***	***H*$_V$**	**Reference**
***hP*10-WB_4**	*P*6_3*/mmc*	exp	262.5(2)	227(2)	1.16(1)	482(30)	37.3(5)	This work - single crystal
		exp	262.5(2)	214(5)	1.23(3)	551(24)	33.3(1.5)	This work - polycrystal
		calc	294	215	1.367	519	$28–35^a$	17
		calc	292	213	1.371	514	21.3^b	88
		calc	299	217	1.378	525	29.0^a	31
		calc	302	259	1.166	604	40.0^a	36
		calc	297	217	1.372	523	28.8^c	37
***hP*15-WB_4**	*R*-3*m*	calc	299	137	2.182	356	11.3^a	31
		calc	308	253	1.217	596	$37–42^a$	17
***hP*20-WB_4**	*P*6_3*/mmc*	exp	304(10)				$46.2(1.2)^f$	26
		exp	339(3)			553(14)	$43.3(2.9)^f$	44
		calc	392	104			41.1^d	43
		calc	328	129	2.543	325		29
		calc	300	102	2.941	274	5.2^a	89
		calc	298	85	3.506	233	3.2^a	31
$WB_{4.2}$	*P*6_3*/mmc*	calc	280	245	1.143	569	39.7^e	54
WB_5	*Pmmn*	calc	287	267	1.075	611	44.9^a	36
		calc	295	270	1.093	621	44.7^e	54
WB_{5-x}–WB_2 (50/50%)		exp					$29.3(2.3)^f$	90
WB_{5-x}–WB_2 (67/33%)		exp					$38.7(1.1)^f$	90

Calculated using the empirical models of: *a* – Chen[85], *b* – Šimůnek[91], *c* – Tian[92], *d* – Gao[93], *e* – Mazhnik–Oganov[94]; *f* – experimental hardness measured at applied load of 0.49 N.

Conclusions

We have successfully synthesized single crystals of the predicted but so far "elusive" stoichiometric WB_4 phase, determined its crystal structure by single-crystal X-ray diffraction and investigated mechanical properties. A hexagonal crystal structure of stoichiometric tungsten tetraboride is formed by single hexagonal close-packed layers of tungsten atoms, which interchange with covalently-bonded boron two-layer networks with short B-B bonds along *c*-axis. The latter bonds contribute to the anisotropic character of axial compressibility. Our single-crystal diffraction data suggest that tungsten atoms fully occupy their crystallographic positions, while, no additional interstitial boron atoms with partial occupancy could be identified. *In situ* high-pressure study shows that a bulk modulus of WB_4 is 238.6(2) GPa. Measurements of mechanical properties on bulk polycrystalline samples at ambient conditions reveal hardness of ~36 GPa. Our work solved the long-standing challenge of the "WB_4" phase and confirmed its high technological potential as a hard material. Further enhance of its mechanical properties could be achieved by alloying with other elements, as it was demonstrated on a non-stoichiometric polymorph of $WB_{4.2}$[44,47]. This phase allows hosting a wide variety of transition metals in its structure forming ternary alloys. As a result, its own Vickers microindentation hardness can increase from ~43 GPa to 51-56 GPa by addition of 6-8% of Ti, Zr or Hf[95] and to 53-54 GPa by addition of 2-10 at.% of Ta, Mn or Cr[96] (the values were measured under an applied load of 0.49 N). Incorporation of group III transition metals (Y, Sc) and selected lanthanoids (Gd, Tb, Dy, Ho, Er) also improves hardness values and oxidation resistance[97].

Author Contributions

Elena Bykova: investigation, conceptualization, formal analysis, funding acquisition, writing – original draft; Sergey V. Ovsyannikov: investigation, formal analysis, writing – original draft; Maxim Bykov: investigation, writing – review & editing; Yuqing Yin: investigation; Timofey Fedotenko: investigation, data curation; Hendrik Holz: investigation, formal analysis; Stefan Gabel: investigation, formal analysis; Benoit Merle: investigation, formal analysis, writing – original draft; Stella Chariton: investigation, data curation; Vitali B. Prakapenka: investigation, data curation, methodology, writing – review & editing; Natalia Dubrovinskaia: resources, writing – review & editing; Alexander F. Goncharov: resources, writing – review & editing; Leonid Dubrovinsky: funding acquisition, resources, writing – review & editing.

Conflicts of interest

There are no conflicts to declare.

Acknowledgements

E.B, M.B. and A.F.G. acknowledge support of the Carnegie Institution of Washington. M.B. acknowledges the support of Deutsche Forschungsgemeinschaft (DFG project BY112/2-1). Portions of this work were performed at GeoSoilEnviroCARS (The University of Chicago, Sector 13), Advanced Photon Source (APS), Argonne National Laboratory. GeoSoilEnviroCARS is supported by the National Science Foundation - Earth Sciences (EAR – 1634415). This research used resources of the Advanced Photon Source, a U.S. Department of Energy (DOE) Office of Science User Facility operated for the DOE Office of Science by Argonne National Laboratory under Contract No. DE-AC02-06CH11357. This research used resources from the Center for Nanoanalysis and Electron Microscopy (CENEM) at Friedrich-Alexander University Erlangen-Nürnberg.

References

1 Y. Liang, X.-F. Wei, C. Gu, J.-X. Liu, F. Li, M. Yan, X. Zheng, Z. Han, Y. Zhao, S. Wang, J. Yang, W. Zhang, L. Kou and G.-J. Zhang, *ACS Appl. Mater. Interfaces*, 2021, **13**, 14365–14376.

2 A. Zerr, R. Riedel, T. Sekine, J. E. Lowther, W. Y. Ching and I. Tanaka, *Adv. Mater.*, 2006, **18**, 2933–2948.

3 A. Zerr, G. Miehe, G. Serghiou, M. Schwarz, E. Kroke, R. Riedel, H. Fueß, P. Kroll and R. Boehler, *Nature*, 1999, **400**, 340–342.

4 K. Watanabe, T. Taniguchi and H. Kanda, *Nat. Mater.*, 2004, **3**, 404–409.

5 S. Vogel, A. T. Buda and W. Schnick, *Angew. Chemie Int. Ed.*, 2018, **57**, 13202–13205.

6 P. Wang, S. Wang, Y. Zou, J. Zhu, D. He, L. Wang and Y. Zhao, *Crystals*, 2021, **11**, 614.

7 M. Bykov, S. Chariton, H. Fei, T. Fedotenko, G. Aprilis, A. V. Ponomareva, F. Tasnádi, I. A. Abrikosov, B. Merle, P. Feldner, S. Vogel, W. Schnick, V. B. Prakapenka, E. Greenberg, M. Hanfland, A. Pakhomova, H.-P. Liermann, T. Katsura, N. Dubrovinskaia and L. Dubrovinsky, *Nat. Commun.*, 2019, **10**, 2994.

8 M. Bykov, E. Bykova, A. V. Ponomareva, I. A. Abrikosov, S. Chariton, V. B. Prakapenka, M. F. Mahmood, L. Dubrovinsky and A. F. Goncharov, *Angew. Chemie Int. Ed.*, 2021, **60**, 9003–9008.

9 B. Albert, *Angew. Chemie Int. Ed.*, 1998, **37**, 1117–1118.

10 H. Gou, L. Hou, J. Zhang, H. Li, G. Sun and F. Gao, *Appl. Phys. Lett.*, 2006, **88**, 221904.

11 B. Petermüller, C. Neun, K. Wurst, L. Bayarjargal, D. Zimmer, W. Morgenroth, M. Avalos-Borja, I. G. Becerril-Juarez, M. J. Mühlbauer, B. Winkler and H. Huppertz, *Inorg. Chem.*, 2018, **57**, 10341–10351.

12 B. Petermüller, C. Neun, M. Stekiel, D. Zimmer, M. Tribus, K. Wurst, B. Winkler and H. Huppertz, *Chem. - A Eur. J.*, 2018, **24**, 14679–14685.

13 C. Neun, B. Petermüller, E. Haussühl, L. Bayarjargal, K. Wurst, T. Götsch, S. Penner, W. Morgenroth, I. G. Becerril-Juarez, M. Avalos-Borja, H. Huppertz and B. Winkler, *Solid State Sci.*, 2020, **105**, 106211.

14 H. Tang, X. Gao, J. Zhang, B. Gao, W. Zhou, B. Yan, X. Li, Q. Zhang, S. Peng, D. Huang, L. Zhang, X. Yuan, B. Wan, C. Peng, L. Wu, D. Zhang, H. Liu, L. Gu, F. Gao, T. Irifune, R. Ahuja, H.-K. K. Mao and H. Gou, *Chem. Mater.*, 2020, **32**, 459–467.

15 B. Zhao, X. Wang, L. Yu, Y. Liu, X. Chen, B. Yang, G. Yang, S. Zhang, L. Gu and X. Liu, *Adv. Funct. Mater.*, 2022, **32**, 2110872.

16 H.-Y. Chung, M. B. Weinberger, J.-M. Yang, S. H. Tolbert and R. B. Kaner, *Appl. Phys. Lett.*, 2008, **92**, 261904.

17 H. Gou, Z. Li, H. Niu, F. Gao, J. Zhang, R. C. Ewing and J. Lian, *Appl. Phys. Lett.*, 2012, **100**, 111907.

18 H. Gou, N. Dubrovinskaia, E. Bykova, A. A. Tsirlin, D. Kasinathan, W. Schnelle, A. Richter, M. Merlini, M. Hanfland, A. M. Abakumov, D. Batuk, G. Van Tendeloo, Y. Nakajima, A. N. Kolmogorov and L. Dubrovinsky, *Phys. Rev. Lett.*, 2013, **111**, 157002.

19 A. Knappschneider, C. Litterscheid, D. Dzivenko, J. A. Kurzman, R. Seshadri, N. Wagner, J. Beck, R. Riedel and B. Albert, *Inorg. Chem.*, 2013, **52**, 540–542.

20 A. Knappschneider, C. Litterscheid, N. C. George, J. Brgoch, N. Wagner, J. Beck, J. A. Kurzman, R. Seshadri and B. Albert, *Angew. Chem. Int. Ed. Engl.*, 2014, **53**, 1684–1688.

21 H. Gou, A. A. Tsirlin, E. Bykova, A. M. Abakumov, G. Van Tendeloo, A. Richter, S. V. Ovsyannikov, A. V. Kurnosov, D. M. Trots, Z. Konôpková, H.-P. Liermann, L. Dubrovinsky and N. Dubrovinskaia, *Phys. Rev. B*, 2014, **89**, 064108.

22 E. Bykova, A. A. Tsirlin, H. Gou, L. Dubrovinsky and N. Dubrovinskaia, *J. Alloys Compd.*, 2014, **608**, 69–72.

23 G. Akopov, M. T. Yeung and R. B. Kaner, *Adv. Mater.*, 2017, **29**, 1604506.

24 S. B. Schneider, D. Baumann, A. Salamat, Z. Konôpková, H.-P. Liermann, M. R. Schwarz, W. Morgenroth, L. Bayarjargal, A. Friedrich, B. Winkler and W. Schnick, *Chem. Mater.*, 2012, **24**, 3240–3246.

25 B. Fuchs, D. Johrendt, L. Bayarjargal and H. Huppertz, *Angew. Chemie Int. Ed.*, 2021, **60**, 21801–21806.

26 Q. Gu, G. G. Krauss and W. Steurer, *Adv. Mater.*, 2008, **20**, 3620–3626.

27 G. Akopov, L. E. Pangilinan, R. Mohammadi and R. B. Kaner, *APL Mater.*, 2018, **6**, 070901.

28 Z. Zhang, A. Mansouri Tehrani, A. O. Oliynyk, B. Day and J. Brgoch, *Adv. Mater.*, 2021, **33**, 2005112.

29 E. Zhao, J. Meng, Y. Ma and Z. Wu, *Phys. Chem. Chem. Phys.*, 2010, **12**, 13158.

30 Q. Tao, D. Zheng, X. Zhao, Y. Chen, Q. Li, Q. Li, C. Wang, T. Cui, Y. Ma, X. Wang and P. Zhu, *Chem. Mater.*, 2014, **26**, 5297–5302.

31 X.-Y. Cheng, X.-Q. Chen, D.-Z. Li and Y.-Y. Li, *Acta Crystallogr. Sect. C Struct. Chem.*, 2014, **70**, 85–103.

32 T. Moscicki, J. Radziejewska, J. Hoffman, J. Chrzanowska, N. Levintant-Zayonts, D. Garbiec and Z. Szymanski, *Ceram. Int.*, 2015, **41**, 8273–8281.

33 N. G. Szwacki, *Sci. Rep.*, 2017, **7**, 1–6.

34 A. G. Kvashnin, H. A. Zakaryan, C. Zhao, Y. Duan, Y. A. Kvashnina, C. Xie, H. Dong and A. R. Oganov, *J. Phys. Chem. Lett.*, 2018, **9**, 3470–3477.

35 Z. Qin, W. Gong, X. Song, M. Wang, H. Wang and Q. Li, *RSC Adv.*, 2018, **8**, 35664–35671.

36 C. Zhao, Y. Duan, J. Gao, W. Liu, H. H. Dong, H. H. Dong, D. Zhang and A. R. Oganov, *Phys. Chem. Chem. Phys.*, 2018, **20**, 24665–24670.

37 A. Yang, Y. Duan, M. Peng, L. Shen and H. Qi, *Appl. Phys. A*, 2022, **128**, 152.

38 A. Chretien and J. Helgorsky, *CR (East Lansing, Mich)*, 1961, **252**, 742–744.

39 P. A. Romans and M. P. Krug, *Acta Crystallogr.*, 1966, **20**, 313–315.

40 J. Dong, H. Li, J. Wang, Z. Guo, J. Liao, X. Hao, X. Zhang and D. Chen, *J. Phys. Chem. C*, 2019, **123**, 29314–29323.

41 Y. Wang, Y. Wu, Y. Lu, X. Wang, Y. Duan and M. Peng, *Vacuum*, 2022, **196**, 110731.

42 I. Zeiringer, P. Rogl, A. Grytsiv, J. Polt, E. Bauer and G. Giester, *J. Phase Equilibria Diffus.*, 2014, **35**, 384–395.

43 M. Wang, Y. Li, T. Cui, Y. Ma and G. Zou, *Appl. Phys. Lett.*, 2008, **93**, 101905.

44 R. Mohammadi, A. T. Lech, M. Xie, B. E. Weaver, M. T. Yeung, S. H. Tolbert and R. B. Kaner, *Proc. Natl. Acad. Sci.*, 2011, **108**, 10958–10962.

45 J. V. Rau, A. Latini, R. Teghil, A. De Bonis, M. Fosca, R. Caminiti and V. Rossi Albertini, *ACS Appl. Mater. Interfaces*, 2011, **3**, 3738–3743.

46 X.-L. Wu, X.-L. Zhou and J. Chang, *Int. J. Mod. Phys. B*, 2015, **29**, 1550103.

47 A. T. Lech, C. L. Turner, R. Mohammadi, S. H. Tolbert and R. B. Kaner, *Proc. Natl. Acad. Sci.*, 2015, **112**, 3223–3228.

48 X. Li, Y. Tao and F. Peng, *J. Alloys Compd.*, 2016, **687**, 579–585.

49 G. Akopov, M. T. Yeung, I. Roh, Z. C. Sobell, H. Yin, W. H. Mak, S. I. Khan and R. B. Kaner, *Chem. Mater.*, 2018, **30**, 3559–3570.

50 H. Gou, Z. Li, L.-M. Wang, J. Lian and Y. Wang, *AIP Adv.*, 2012, **2**, 012171.

51 X. Cheng, W. Zhang, X.-Q. Chen, H. Niu, P. Liu, K. Du, G. Liu, D. Li, H.-M. Cheng, H. Ye and Y. Li, *Appl. Phys. Lett.*, 2013, **103**, 171903.

52 E. M. Carnicom, J. Strychalska-Nowak, P. Wiśniewski, D. Kaczorowski, W. Xie, T. Klimczuk and R. J. Cava, *Supercond. Sci. Technol.*, 2018, **31**, 115005.

53 W. Gong, C. Liu, X. Song, Q. Li, Y. Ma and C. Chen, *Phys. Rev. B*, 2019, **100**, 220102.

54 A. G. Kvashnin, D. V. Rybkovskiy, V. P. Filonenko, V. I. Bugakov, I. P. Zibrov, V. V. Brazhkin, A. R. Oganov, A. A. Osiptsov and A. Y. Zakirov, *Adv. Sci.*, 2020, **7**, 2000775.

55 C. Gu, Y. Liang, X. Zhou, J. Chen, D. Ma, J. Qin, W. Zhang, Q. Zhang, L. L. Daemen, Y. Zhao and S. Wang, *Phys. Rev. B*, 2021, **104**, 014110.

56 K. D. Shumilov, Z. Mehmedović, H. Yin, P. Poths, S. Nuryyeva, I. Liepuoniute, C. Jang, I. Winardi and A. N. Alexandrova, *J. Phys. Chem. C*, 2021, **125**, 9486–9496.

57 F. Cardarelli, *Materials Handbook. A Concise Desktop Reference*, Springer London, London, 2nd edn., 2008.

58 H. Nowotny, H. Haschke and F. Benesovsky, *Monatshefte für Chemie - Chem. Mon.*, 1967, **98**, 547–554.

59 T. Lundström and I. Rosenberg, *J. Solid State Chem.*, 1973, **6**, 299–305.

60 R. Letoullec, J. P. Pinceaux and P. Loubeyre, *High Press. Res.*, 1988, **1**, 77–90.

61 Y. Fei, A. Ricolleau, M. Frank, K. Mibe, G. Shen and V. Prakapenka, *Proc. Natl. Acad. Sci. U. S. A.*, 2007, **104**, 9182–9186.

62 V. B. Prakapenka, A. Kubo, A. Kuznetsov, A. Laskin, O. Shkurikhin, P. Dera, M. L. Rivers and S. R. Sutton, *High Press. Res.*, 2008, **28**, 225–235.

63 D. L. Heinz and R. Jeanloz, in *High-Pressure Research in Mineral Physics: A Volume in Honor of*

Syun-iti Akimoto, Volume 39, eds. M. H. Manghnani and Y. Syono, Terra Scientific Publishing, 1987, pp. 113–127.

64 C. Prescher and V. B. Prakapenka, *High Press. Res.*, 2015, **35**, 223–230.

65 V. Petříček, M. Dušek and L. Palatinus, *Zeitschrift für Krist. - Cryst. Mater.*, 2014, **229**, 345–352.

66 D. . Frost, B. . Poe, R. . Trønnes, C. Liebske, A. Duba and D. . Rubie, *Phys. Earth Planet. Inter.*, 2004, **143–144**, 507–514.

67 S. V Ovsyannikov, M. Bykov, S. A. Medvedev, P. G. Naumov, A. Jesche, A. A. Tsirlin, E. Bykova, I. Chuvashova, A. E. Karkin, V. Dyadkin, D. Chernyshov and L. S. Dubrovinsky, *Angew. Chemie Int. Ed.*, 2020, **59**, 5632–5636.

68 S. V. Ovsyannikov, H. Gou, A. E. Karkin, V. V. Shchennikov, R. Wirth, V. Dmitriev, Y. Nakajima, N. Dubrovinskaia and L. S. Dubrovinsky, *Chem. Mater.*, 2014, **26**, 5274–5281.

69 *CrysAlisPro Softw. Syst. version 1.171.40.84a, Rigaku Oxford Diffraction, Oxford, UK.*

70 G. M. Sheldrick, *Acta Crystallogr. Sect. A Found. Adv.*, 2015, **71**, 3–8.

71 G. M. Sheldrick, *Acta Crystallogr. Sect. C Struct. Chem.*, 2015, **71**, 3–8.

72 O. V. Dolomanov, L. J. Bourhis, R. J. Gildea, J. A. K. Howard and H. Puschmann, *J. Appl. Crystallogr.*, 2009, **42**, 339–341.

73 B. Merle, V. Maier-Kiener and G. M. Pharr, *Acta Mater.*, 2017, **134**, 167–176.

74 P. Sudharshan Phani and W. C. Oliver, *Mater. Des.*, 2019, **164**, 107563.

75 W. C. Oliver and G. M. Pharr, *J. Mater. Res.*, 1992, **7**, 1564–1583.

76 W. C. Oliver and G. M. Pharr, *J. Mater. Res.*, 2004, **19**, 3–20.

77 *Metallic materials—Instrumented indentation test for hardness and materials parameters—Part 1: Test method. Int. Stand. ISO 14577–1*, 2002.

78 R. Kiessling, A. Wetterholm, L. G. Sillén, A. Linnasalmi and P. Laukkanen, *Acta Chem. Scand.*, 1947, **1**, 893–916.

79 M. Kayhan, E. Hildebrandt, M. Frotscher, A. Senyshyn, K. Hofmann, L. Alff and B. Albert, *Solid State Sci.*, 2012, **14**, 1656–1659.

80 M. Frotscher, W. Klein, J. Bauer, C.-M. Fang, J.-F. Halet, A. Senyshyn, C. Baehtz and B. Albert, *Zeitschrift für Anorg. und Allg. Chemie*, 2007, **633**, 2626–2630.

81 J. C. Jamieson, *Science*, 1963, **139**, 1291–1292.

82 H.-Y. Y. Chung, M. B. Weinberger, J. B. Levine, A. Kavner, J.-M. M. Yang, S. H. Tolbert and R. B. Kaner, *Science*, 2007, **316**, 436–439.

83 M. Xie, R. Mohammadi, Z. Mao, M. M. Armentrout, A. Kavner, R. B. Kaner and S. H. Tolbert, *Phys. Rev. B - Condens. Matter Mater. Phys.*, 2012, **85**, 1–8.

84 D. M. Teter, *MRS Bull.*, 1998, **23**, 22–27.

85 X. Q. Chen, H. Niu, D. Li and Y. Li, *Intermetallics*, 2011, **19**, 1275–1281.

86 X.-Q. Chen, H. Niu, C. Franchini, D. Li and Y. Li, *Phys. Rev. B*, 2011, **84**, 121405.

87 S. F. Pugh, *London, Edinburgh, Dublin Philos. Mag. J. Sci.*, 1954, **45**, 823–843.

88 M. Zhang, H. Yan, Q. Wei and H. Wang, *Comput. Mater. Sci.*, 2013, **68**, 371–378.

89 Y. Liang, Z. Fu, X. Yuan, S. Wang, Z. Zhong and W. Zhang, *EPL (Europhysics Lett.*, 2012, **98**, 66004.

90 A. Y. Pak, D. V. Rybkovskiy, Y. Z. Vassilyeva, E. N. Kolobova, A. V. Filimonenko and A. G. Kvashnin, *Inorg. Chem.*, 2022, **61**, 6773–6784.

91 A. Šimůnek and J. Vackář, *Phys. Rev. Lett.*, 2006, **96**, 085501.

92 Y. Tian, B. Xu and Z. Zhao, *Int. J. Refract. Met. Hard Mater.*, 2012, **33**, 93–106.

93 F. Gao, J. He, E. Wu, S. Liu, D. Yu, D. Li, S. Zhang and Y. Tian, *Phys. Rev. Lett.*, 2003, **91**, 015502.

94 E. Mazhnik and A. R. Oganov, *J. Appl. Phys.*, 2019, **126**, 125109.

95 G. Akopov, M. T. Yeung, C. L. Turner, R. Mohammadi and R. B. Kaner, *J. Am. Chem. Soc.*, 2016, **138**, 5714–5721.

96 M. Xie, R. Mohammadi, C. L. Turner, R. B. Kaner, A. Kavner and S. H. Tolbert, *Appl. Phys. Lett.*, , DOI:10.1063/1.4927596.

97 G. Akopov, M. T. Yeung, I. Roh, Z. C. Sobell, H. Yin, W. H. Mak, S. I. Khan and R. B. Kaner, *Chem. Mater.*, 2018, **30**, 3559–3570.